electronics

MDPI

Article

Rapid Beam Tracking Using Power Measurement for Terahertz Communications

Xiaodan He [1], Changming Zhang [1,*], Chi Lu [2] and Xianbin Yu [3]

[1] Research Center for Novel Computating Sensing and Intelligent Processing, Zhejiang Lab, Hangzhou 311121, China; hexd@zhejianglab.com
[2] Research Center for High Efficiency Computing System, Zhejiang Lab, Hangzhou 311121, China; luchi@zhejianglab.com
[3] College of Information Science and Electronic Engineering, Zhejiang University, Hangzhou 310027, China; xyu@zju.edu.cn
* Correspondence: zhangcm@zhejianglab.com

Abstract: With abundant bandwidth resources, terahertz communications are considered one of the key technologies to meet the requirement for high data-rate transmission in the future. In order to compensate for the severe propagation loss of terahertz communications, directional antennas with high gain and narrow beams are expected to be adopted, making beam tracking significant for robust communications. In this paper, a tracking method based on power measurement is proposed, consisting of beam status monitoring, recognition of the deviation direction, and movement toward the optimal angle. By observing the change in the received signal power, beam misalignment is first checked, and whether the misalignment is out of tracking range is also determined. Then, the deviation direction is recognized by comparing the received power variations in the candidate directions, and the beam angle is adjusted accordingly until it reaches the optimal angle. With a small scanning range, the deviation direction is recognized in a short duration, allowing for rapid beam tracking. Numerical results indicate that the alignment error is competitively low and stable in the proposed beam tracking method, and its technical superiority is particularly dominant in situations involving variable motion at high speeds.

Keywords: terahertz communications; beam tracking; power measurement; recognition of deviation direction

check for updates

Citation: He, X.; Zhang, C.; Lu, C.; Yu, X. Rapid Beam Tracking Using Power Measurement for Terahertz Communications. *Electronics* **2024**, *13*, 2129. https://doi.org/10.3390/electronics13112129

Academic Editor: Adão Silva

Received: 16 April 2024
Revised: 16 May 2024
Accepted: 18 May 2024
Published: 29 May 2024

Copyright: © 2024 by the authors. Licensee MDPI, Basel, Switzerland. This article is an open access article distributed under the terms and conditions of the Creative Commons Attribution (CC BY) license (https://creativecommons.org/licenses/by/4.0/).

1. Introduction

With huge contiguous bandwidths of up to tens or even hundreds of GHz, terahertz communications are considered one of the key technologies to meet the requirement for high data-rate transmission in the future [1,2]. Due to high frequencies ranging from 0.1 THz to 10 THz, terahertz communications suffer from severe propagation loss according to deterministic or statistical channel models [3]. Directional antennas with high gain and narrow beams are expected to be adopted, especially when the communication distance is long [4]. With these antennas, slight beam misalignment can cause significant degradation in link stability and even result in communication outages [5,6]. Therefore, beam misalignment becomes one of the main bottlenecks for terahertz communications [7,8].

To resolve the beam misalignment issue, a great deal of research has been carried out, with angle-of-arrival (AoA) estimation and beam search being the two main methods. The AoA estimation method is conducted using the observations of different beamforming coefficients or beam angles. The estimation algorithms include the multiple signal classification (MUSIC) algorithm [9,10], power-weighted method [11], deep learning-based technique [12,13], etc. The beam search method selects from candidate angles to find the beam angle that optimizes a certain objective, e.g., maximizing the received signal power. An exhaustive search was applied in [14], and some hierarchical searching techniques were

proposed based on both wide beams and narrow beams in [15–17]. For mobile scenarios, beam tracking should always be carried out after successful beam alignment to continuously maintain the aligned status. Although existing AoA estimation and beam search methods can be adopted for beam tracking, given that they need to be performed frequently to adjust the beam angle, the sounding overhead for testing different beamforming coefficients or beam angles, as well as the computational overhead due to calculation complexity, is considerably high, especially for motion scenarios at high speeds [18,19].

In order to reduce the overhead, some improved methods have been proposed for beam tracking. Instead of performing sounding at a fixed frequency, event-based tracking schemes were proposed to dynamically adjust the sounding interval [15,20,21]. Furthermore, the optimal beam angle was predicted based on the motion parameters estimated from previous observations [21], and dynamic beamwidth adjustment was employed to adapt to channel uncertainty [20,22], thereby reducing the frequency of sounding. However, the beamwidth adaption method requires sophisticated hardware to change the width of a beam in addition to the angle. For each sounding, the number of tested beamforming coefficients or beam angles could be reduced through prediction algorithms based on the angle [15,22–25] and position [26,27], probability-based selections [28,29], Kalman filter methods [30], machine learning techniques [12,31], and utilizing the sensing information from mathematical processing or sensors [32–34]. However, the scanning range of the search method still needs to cover the optimal angle. For the AoA estimation method, in order to reduce the computational complexity, a subspace tracking scheme was studied in [9] to avoid the eigenvalue decomposition within MUSIC algorithms, and a Kalman filter-based method with a small-sized covariance matrix was designed to reduce the calculation complexity of the matrix inverse [35]. However, the computational complexity still cannot meet the requirement for low-complexity implementation in practice.

In this paper, we develop a search method and propose a novel beam tracking scheme with a small scanning range. Power measurement is used to indicate the status of the beam alignment. When the beam is not aligned, the deviation direction, rather than the AoA, is determined by testing candidate directions within a small scanning range and comparing the corresponding received power variations. Then, the beam angle is adjusted accordingly until it reaches the optimal position. With a small scanning range, the sounding overhead is low, and the deviation direction can be recognized in a short duration, allowing the optimal angle to be reached quickly with a single scanning direction, enabling rapid beam tracking. Furthermore, compared with estimation methods such as the MUSIC algorithms or Kalman-filter-based methods, the deviation direction is recognized through comparison, and there is no complicated computation, so beam tracking can be realized with low computational overhead. Consequently, our proposed method is quite suitable for terahertz communications, where beam tracking needs to be performed frequently because of the high sensitivity to imperfect beam alignment. Simulation results verify the performance of the proposed beam tracking method in terms of the alignment error, which is competitively low and stable, and its technical superiority is particularly dominant in situations involving variable motion at high speeds.

The rest of this paper is organized as follows. Section 2 introduces the system model. Section 3 provides the proposed beam tracking method in detail. Section 4 presents the numerical results. Finally, Section 5 concludes this paper.

2. System Model

We consider a point-to-point terahertz communications system with the ability to calculate the received power. Although large-scale antenna arrays can be applied to achieve high beamforming gain, the beamforming architecture and the corresponding codebooks need to be designed elaborately [36]. With low complexity, a single directional antenna is considered in this paper. It should be noted that the proposed beam tracking method is also applicable to antenna arrays because antenna arrays with fixed beam patterns can

be regarded as a single antenna. For the propagation path, the line-of-sight (LoS) path is considered, which is the dominant component of the terahertz channel [4].

According to the Friis transmission equation, the power of the received signal suffering from free-space path loss can be expressed as

$$P_{\mathrm{rx}} = P_{\mathrm{tx}} + G_{\mathrm{tx}} + G_{\mathrm{rx}} - 10 \cdot \log_{10} \frac{c^2}{(4\pi r f)^2}, \tag{1}$$

where P_{tx} is the transmitted power in dBm; G_{tx} and G_{rx} are the antenna gains at the transmitter and receiver, respectively; c is the speed of light; r is the distance between the transmitter and receiver; and f is the carrier frequency. In the case of perfect beam alignment, G_{tx} and G_{rx} reach the maximum values $G_{\mathrm{tx}}^{\max}$ and $G_{\mathrm{rx}}^{\max}$, respectively, and the optimal signal quality is achieved.

For mobile scenarios where the position of the transmitter or receiver changes, G_{tx} and G_{rx} will decrease if the beam angle cannot adjust accordingly. In this paper, we only consider the azimuth angle changing within the horizontal plane, and the transmitter beam is always aligned for simplicity. For changes in the elevation angle, the beam tracking method proposed in this paper can be easily extended by adjusting the beam angle within the elevation plane. For combined transmitter and receiver beam tracking, the proposed beam tracking method can also be extended by performing adjustments at both the transmitter and receiver alternately. Let θ_n^{opt} denote the optimal beam angle of the receiver at time instant t_n, θ_n^{act} denote the actual beam angle, and $\epsilon_n = \theta_n^{\mathrm{act}} - \theta_n^{\mathrm{opt}}$ denote the alignment error. Then, the received signal power can be rewritten as

$$P_{\mathrm{rx}}(n) = P_{\mathrm{tx}} + G_{\mathrm{tx}}^{\max} + G_{\mathrm{rx}}(\epsilon_n) - 10 \cdot \log_{10} \frac{c^2}{(4\pi r_n f)^2}, \tag{2}$$

where r_n is the distance at instant t_n and the transmitted power P_{tx} used for beam tracking is assumed to be constant.

It should be noted that the power of the received signal is related to the beam alignment error and the distance between the transmitter and receiver. For terahertz communications systems equipped with narrow beam antennas, the antenna gain is quite sensitive to beam misalignment, the impact of which is dominant on the received signal power, especially for long-distance scenarios. For example, considering an initial distance of 1000 m between the transmitter and receiver, and referring to a commercial terahertz Cassegrain antenna [37], for which the beam pattern is illustrated in Figure 1 and the half-power beamwidth (HPBW) is 0.2 degrees, when the receiver moves 1.7 m away vertically from the initial direction from the transmitter to the receiver, the beam alignment error changes by 0.1 degrees and the antenna gain decreases by 3 dB, while the path loss change due to distance is only 10^{-5} dB.

In addition to the power of the received signal, the power measurement obtained at the receiver includes the impact of noise. Considering that the beam tracking procedure is applied after a successful beam alignment, the signal-to-noise ratio at the receiver is high enough to support high data-rate transmission, so the power measurement with noise is approximately equal to that without noise.

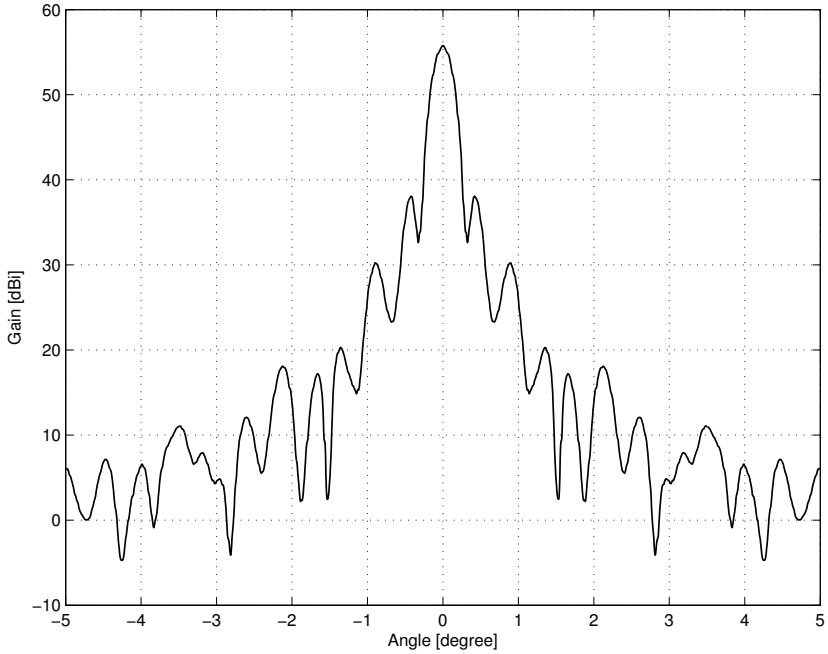


Figure 1. Beam pattern example [37].

3. Proposed Beam Tracking Method

In this section, we present an overview of the beam tracking procedure. We introduce each component in detail, including beam status monitoring, recognition of the deviation direction, and movement toward the optimal angle.

3.1. Overview of Beam Tracking Procedure

In order to narrow down the scanning range of candidate directions to reduce the sounding overhead and improve efficiency, we propose a novel beam tracking procedure using power measurement. Figure 2 shows a block diagram in which beam training for initial beam alignment is mentioned for completeness. Considering that beam tracking is applied after successful beam alignment through beam training, our proposed procedure starts with beam status monitoring by observing the received power to check whether the optimal beam angle has changed, which means that the current beam angle is no longer optimal. Until the optimal angle changes, beam status monitoring continues, and other components are not triggered. When the checking result shows that the optimal angle has changed, beam status monitoring additionally determines whether the optimal beam angle is out of the tracking range, which indicates the tracking ability of this procedure. If it is, the beam tracking procedure is interrupted, and beam training with a wider scanning range should be performed. Otherwise, the beam tracking procedure continues, and the deviation direction is recognized, through testing candidate directions and comparing the corresponding received power variations. The recognition result of the deviation direction can be none, clockwise, or anticlockwise, which means that the beam does not need to be rotated or should be turned clockwise or anticlockwise, respectively. Then, the beam angle is adjusted accordingly until the optimal angle is reached, followed by repeated beam tracking procedures starting with beam status monitoring.

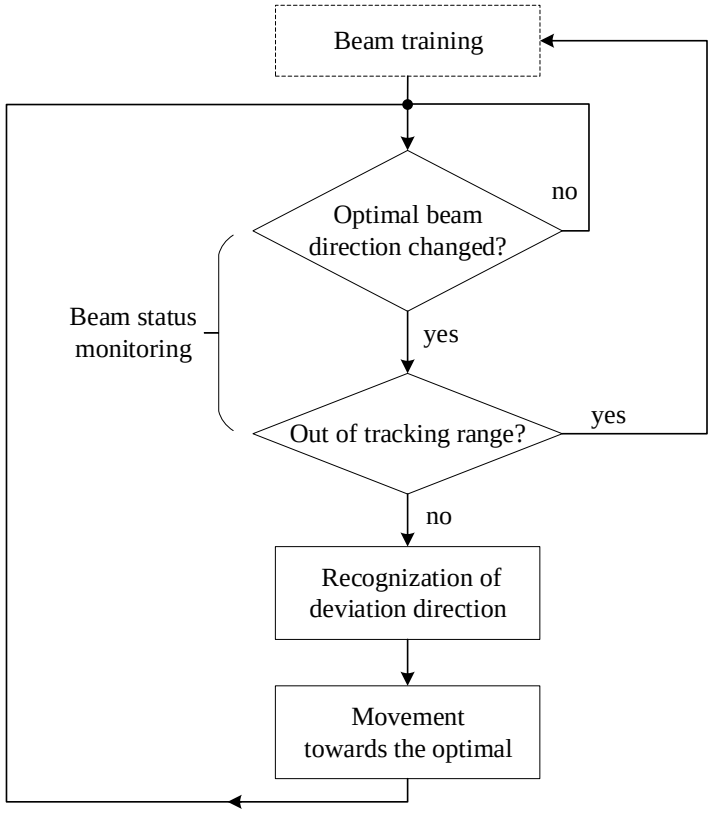


Figure 2. Block diagram of the proposed beam tracking procedure.

3.2. Beam Status Monitoring

As presented in Section 2, the power of the received signal is related to the beam alignment error and the distance between the transmitter and receiver. The impact of beam misalignment is significant for terahertz communications systems equipped with narrow beam antennas. Therefore, the received power can be used to indicate the beam alignment status. In this paper, the horizontal plane is divided into small and equal angular intervals μ. Correspondingly, the actual angle of the beam can be adjusted in several steps, with the angle change of each step equal to μ. In order to achieve beam tracking, the adjustment speed of the actual angle should be high enough to keep up with changes in the optimal angle.

On the one hand, when the transmitter or receiver is moving from an interval with perfect beam alignment to a neighboring one, the received power will decrease. Let $P_{\mathrm{rx}}^{\mathrm{opt}}$ denote the received signal power with the optimal beam angle. At the beginning of beam tracking, considering that perfect beam alignment has been achieved through beam training, $P_{\mathrm{rx}}^{\mathrm{opt}}$ is initialized to the received power and is updated during the recognition of the deviation direction stage, which is introduced in Section 3.3. Then, the change in the optimal beam angle can be checked by

$$P_{\mathrm{rx}}(n) < P_{\mathrm{rx}}^{\mathrm{opt}} - \rho_0, \tag{3}$$

where ρ_0 denotes the reduction threshold of the received power, which is related to μ, e.g., $\rho_0 = G_{\mathrm{rx}}^{\max} - G_{\mathrm{rx}}(\mu)$.

On the other hand, a tracking range is set to indicate the capability of beam tracking in the proposed method. When the transmitter or receiver moves drastically and out of the tracking range, beam tracking is interrupted, and beam training with a wider scanning range should be performed. In this paper, the beam tracking method is designed based on

the monotonic characteristic of the antenna gain on the main lobe, so the tracking range can be set according to the beamwidth of the main lobe. Similarly, the optimal beam angle being out of the tracking range can be checked through the received power by

$$P_{\mathrm{rx}}(n) < P_{\mathrm{rx}}^{\mathrm{opt}} - \rho_1, \tag{4}$$

where ρ_1 is the power reduction threshold that depends on the tracking range.

3.3. Recognition of Deviation Direction

There are two types of scanning applied to recognize the deviation direction: bidirectional scanning and unidirectional scanning. Bidirectional scanning is performed in two directions with three scanning points $\{\theta_n^{\mathrm{act}}, \theta_{n+1}^{\mathrm{act}}, \theta_{n+2}^{\mathrm{act}}\}$, where θ_n^{act} is the beam angle when the scanning starts. The initial scanning direction, i.e., the direction from θ_n^{act} to $\theta_{n+1}^{\mathrm{act}}$, can be anticlockwise or clockwise. In this paper, it is specifically set to the anticlockwise direction for simplicity; however, it should be noted that when scanning starts in the clockwise direction, the analysis method presented in this paper is still applicable. Then, the other two scanning points can be written as $\theta_{n+1}^{\mathrm{act}} = \theta_n^{\mathrm{act}} + \mu$ and $\theta_{n+2}^{\mathrm{act}} = \theta_{n+1}^{\mathrm{act}} - \mu$. For the initial scanning direction, define $M_{\mathrm{same}}^{\mathrm{double}}$ as the variation in the received signal power, i.e., $P_{\mathrm{rx}}(n+1) - P_{\mathrm{rx}}(n)$, which consists of the antenna gain change and propagation loss change caused by the varying beam alignment error and transceiver distance, respectively. Since the impact of the transceiver distance change on the received power is negligible, as presented in Section 2, $P_{\mathrm{rx}}(n+1) - P_{\mathrm{rx}}(n)$ is approximate to the antenna gain change caused by the varying beam alignment error, i.e., $G_{\mathrm{rx}}(\epsilon_{n+1}) - G_{\mathrm{rx}}(\epsilon_n)$. Furthermore, in order to separate the impact of the optimal angle change and the actual angle change, the term $G_{\mathrm{rx}}\left(\theta_{n+1}^{\mathrm{act}} - \theta_n^{\mathrm{opt}}\right)$ is added and subtracted. Then, $M_{\mathrm{same}}^{\mathrm{double}}$ can be expressed as

$$\begin{aligned} M_{\mathrm{same}}^{\mathrm{double}} &= P_{\mathrm{rx}}(n+1) - P_{\mathrm{rx}}(n) \approx G_{\mathrm{rx}}\left(\theta_{n+1}^{\mathrm{act}} - \theta_{n+1}^{\mathrm{opt}}\right) - G_{\mathrm{rx}}\left(\theta_n^{\mathrm{act}} - \theta_n^{\mathrm{opt}}\right) \\ =& G_{\mathrm{rx}}\left(\theta_{n+1}^{\mathrm{act}} - \theta_{n+1}^{\mathrm{opt}}\right) - G_{\mathrm{rx}}\left(\theta_{n+1}^{\mathrm{act}} - \theta_n^{\mathrm{opt}}\right) + G_{\mathrm{rx}}\left(\theta_{n+1}^{\mathrm{act}} - \theta_n^{\mathrm{opt}}\right) - G_{\mathrm{rx}}\left(\theta_n^{\mathrm{act}} - \theta_n^{\mathrm{opt}}\right), \end{aligned} \tag{5}$$

where the first part $G_{\mathrm{rx}}(\theta_{n+1}^{\mathrm{act}} - \theta_{n+1}^{\mathrm{opt}}) - G_{\mathrm{rx}}(\theta_{n+1}^{\mathrm{act}} - \theta_n^{\mathrm{opt}})$ with the same actual angle indicates the power change caused by the variation in the optimal beam angle, and the second part $G_{\mathrm{rx}}(\theta_{n+1}^{\mathrm{act}} - \theta_n^{\mathrm{opt}}) - G_{\mathrm{rx}}(\theta_n^{\mathrm{act}} - \theta_n^{\mathrm{opt}})$ with the same optimal angle represents the power change caused by the adjustment of the actual beam angle. Similarly, for the reverse direction, i.e., from $\theta_{n+1}^{\mathrm{act}}$ to $\theta_{n+2}^{\mathrm{act}}$, the variation in the received signal power $M_{\mathrm{diff}}^{\mathrm{double}}$ can be expressed as

$$\begin{aligned} M_{\mathrm{diff}}^{\mathrm{double}} &= P_{\mathrm{rx}}(n+2) - P_{\mathrm{rx}}(n+1) \approx G_{\mathrm{rx}}\left(\theta_{n+2}^{\mathrm{act}} - \theta_{n+2}^{\mathrm{opt}}\right) - G_{\mathrm{rx}}\left(\theta_{n+1}^{\mathrm{act}} - \theta_{n+1}^{\mathrm{opt}}\right) \\ =& G_{\mathrm{rx}}\left(\theta_{n+2}^{\mathrm{act}} - \theta_{n+2}^{\mathrm{opt}}\right) - G_{\mathrm{rx}}\left(\theta_{n+2}^{\mathrm{act}} - \theta_{n+1}^{\mathrm{opt}}\right) + G_{\mathrm{rx}}\left(\theta_{n+2}^{\mathrm{act}} - \theta_{n+1}^{\mathrm{opt}}\right) - G_{\mathrm{rx}}\left(\theta_{n+1}^{\mathrm{act}} - \theta_{n+1}^{\mathrm{opt}}\right). \end{aligned} \tag{6}$$

During the scanning period, assuming the changing velocity of the optimal beam angle remains the same and the antenna gain changes linearly corresponding to the varying angle, the first parts of $M_{\mathrm{same}}^{\mathrm{double}}$ and $M_{\mathrm{diff}}^{\mathrm{double}}$ can be regarded as being the same, and $M_{\mathrm{same}}^{\mathrm{double}} - M_{\mathrm{diff}}^{\mathrm{double}}$ can be written as

$$\begin{aligned} M_{\mathrm{same}}^{\mathrm{double}} - M_{\mathrm{diff}}^{\mathrm{double}} =& \left\{ G_{\mathrm{rx}}\left(\theta_{n+1}^{\mathrm{act}} - \theta_n^{\mathrm{opt}}\right) - G_{\mathrm{rx}}\left(\theta_n^{\mathrm{act}} - \theta_n^{\mathrm{opt}}\right) \right\} - \\ & \left\{ G_{\mathrm{rx}}\left(\theta_{n+2}^{\mathrm{act}} - \theta_{n+1}^{\mathrm{opt}}\right) - G_{\mathrm{rx}}\left(\theta_{n+1}^{\mathrm{act}} - \theta_{n+1}^{\mathrm{opt}}\right) \right\}. \end{aligned} \tag{7}$$

Unidirectional scanning is performed in a single direction with two scanning points θ_m^{act} and $\theta_{m+1}^{\mathrm{act}}$, where θ_m^{act} is the point at which unidirectional scanning starts, and $\theta_{m+1}^{\mathrm{act}}$ is equal to $\theta_m^{\mathrm{act}} + \mu$ or $\theta_m^{\mathrm{act}} - \mu$ when the scanning direction is anticlockwise or clockwise,

respectively. The corresponding variation in the received signal power M^{single} is calculated by $M^{\text{single}} = P_{\text{rx}}(m+1) - P_{\text{rx}}(m)$.

In order to recognize the deviation direction, bidirectional scanning is first carried out. The relationship between the optimal angle and the actual angle can be divided into four cases, and unidirectional scanning should be performed subsequently in two cases to confirm the deviation direction. Figure 3 illustrates the scanning schematics when the motion direction is clockwise. The four cases are described as follows:

- In case (a), there is no intersection between the optimal and actual beam angles during bidirectional scanning, and the optimal angle is always larger than the actual angle, which is illustrated in Figure 3a. Compared with θ_n^{act}, $\theta_{n+1}^{\text{act}}$ is closer to θ_n^{opt}, so the second part of $M_{\text{same}}^{\text{double}}$ is positive. Similarly, the second part of $M_{\text{diff}}^{\text{double}}$ is negative. Therefore, the value of $M_{\text{same}}^{\text{double}} - M_{\text{diff}}^{\text{double}}$ is significantly positive, and the beam should be turned anticlockwise to reach the optimal angle, which is the same as the initial scanning direction.
- In case (b), there are intersections between the optimal and actual beam angles during bidirectional scanning, as illustrated in Figure 3b. Since the actual angle is always close to the optimal angle, the value of $M_{\text{same}}^{\text{double}} - M_{\text{diff}}^{\text{double}}$ is approximately zero. In this case, the actual angle does not need to be adjusted, and the deviation direction can be regarded as none.
- In case (c), there is no intersection between the optimal and actual angles of the beam during bidirectional scanning, and the optimal angle is always less than the actual angle but does not deviate significantly from it. Compared with θ_n^{act}, $\theta_{n+1}^{\text{act}}$ is further from θ_n^{opt}, so the second part of $M_{\text{same}}^{\text{double}}$ is negative. Similarly, the second part of $M_{\text{diff}}^{\text{double}}$ is positive, thus $M_{\text{same}}^{\text{double}} - M_{\text{diff}}^{\text{double}}$ is significantly negative. It should be noted that in case (d), this value is also significantly negative. In order to distinguish between these two cases, unidirectional scanning is subsequently applied in a clockwise direction, as illustrated in Figure 3c. In addition to $M_{\text{same}}^{\text{double}} - M_{\text{diff}}^{\text{double}}$, $M_{\text{same}}^{\text{double}} - M^{\text{single}}$ also represents the received power variation in two different scanning directions, but $M_{\text{same}}^{\text{double}} - M^{\text{single}}$ is closer to zero due to the intersection between the optimal and actual angles during unidirectional scanning. In this case, the actual angle of the beam does not need to be adjusted, and the deviation direction can be regarded as none.
- In case (d), the phenomenon is the same as that in case (c) during bidirectional scanning, while the actual angle deviates significantly from the optimal angle, which is illustrated in Figure 3d. Unlike case (c), $M_{\text{same}}^{\text{double}} - M^{\text{single}}$ is approximate to $M_{\text{same}}^{\text{double}} - M_{\text{diff}}^{\text{double}}$. In this case, the beam should be turned clockwise to reach the optimal angle, which is different from the initial scanning direction.

Therefore, the deviation direction can be recognized according to the indicators $M_{\text{same}}^{\text{double}} - M_{\text{diff}}^{\text{double}}$ and $M_{\text{same}}^{\text{double}} - M^{\text{single}}$, both of which are related to the received power variations corresponding to two different scanning directions. Specifically, there are three categories of indicator characteristics, which can be defined by a positive threshold δ_{double}. When $M_{\text{same}}^{\text{double}} - M_{\text{diff}}^{\text{double}}$ or $M_{\text{same}}^{\text{double}} - M^{\text{single}}$ is larger than δ_{double}, it is positive enough. When the value is less than $-\delta_{\text{double}}$, it is negative enough. Otherwise, the indicator is regarded as near zero. It should be noted that with a larger scanning step, δ_{double} should be set to a larger value. The relationship between the indicators and the deviation direction is presented in Table 1.

When the motion direction is anticlockwise, although the detailed schematics are different from those shown in Figure 3, the relationship between the indicators and the deviation direction is the same as that shown in Table 1. As a result, through bidirectional scanning, the deviation direction is anticlockwise when the indicator $M_{\text{same}}^{\text{double}} - M_{\text{diff}}^{\text{double}}$ is larger than δ_{double}, and it is none when the absolute value of this indicator does not exceed δ_{double}. If this indicator is less than $-\delta_{\text{double}}$, unidirectional scanning is subsequently carried out. If the indicator $M_{\text{same}}^{\text{double}} - M^{\text{single}}$ is also less than $-\delta_{\text{double}}$, the deviation direction is clockwise. Otherwise, the deviation direction is estimated as none.

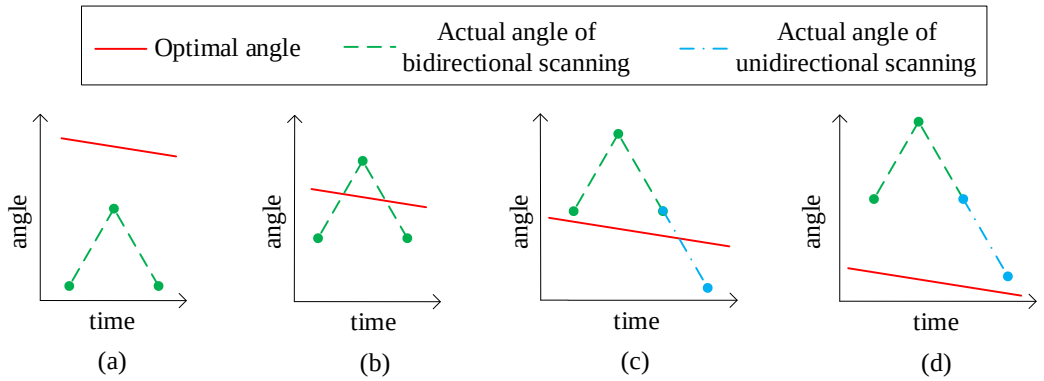


Figure 3. Schematics of the four cases where the motion direction is clockwise: (**a**) The optimal angle is always larger than the actual during bidirectional scanning. (**b**) There are intersections between the optimal and actual angles during bidirectional scanning. (**c**) The optimal angle is always less than the actual during bidirectional scanning, but does not deviate significantly from it. (**d**) The optimal angle is always less than the actual during bidirectional scanning, and deviates significantly from it.

Table 1. Relationship between indicators and deviation direction when the motion direction is clockwise.

Case Index	Indicator 1 $\left(M_{\text{same}}^{\text{double}} - M_{\text{diff}}^{\text{double}}\right)$	Indicator 2 $\left(M_{\text{same}}^{\text{double}} - M^{\text{single}}\right)$	Deviation Direction
(a)	$> \delta_{\text{double}}$	\	anticlockwise
(b)	$\leq \delta_{\text{double}}$ and $\geq -\delta_{\text{double}}$	\	none
(c)	$< -\delta_{\text{double}}$	$\not< -\delta_{\text{double}}$	none
(d)	$< -\delta_{\text{double}}$	$< -\delta_{\text{double}}$	clockwise

Based on the above analysis, the method for recognizing the deviation direction is shown in Algorithm 1, where d_{est} is the estimated deviation direction and $|\cdot|$ represents the absolute value. The possible values of d_{est} are 1, -1, and 0, representing the anticlockwise direction, clockwise direction, and none, respectively. When $d_{\text{est}} = -1$, $M_{\text{diff}}^{\text{double}}$ is updated with M^{single}, and the values of $M_{\text{same}}^{\text{double}}$ and $M_{\text{diff}}^{\text{double}}$ are exchanged with each other so that $M_{\text{same}}^{\text{double}}$ always represents the latest received power variation with the estimated deviation direction, and $M_{\text{diff}}^{\text{double}}$ represents that with the reverse direction, which facilitates the description in the next subsection. Additionally, if the deviation direction is recognized as none through bidirectional scanning, $P_{\text{rx}}^{\text{opt}}$ is updated with the received power of the last scanning points, which are used in the next round of the beam tracking procedures starting with beam status monitoring. It should be noted that the scanning range is a single step only so that the sounding overhead is low, and the deviation direction can be recognized in a short duration.

Algorithm 1 Recognition of deviation direction

Set the initial scanning direction to anticlockwise;
Scan in two different directions and calculate $M_{\text{same}}^{\text{double}}$ and $M_{\text{diff}}^{\text{double}}$;
if $M_{\text{same}}^{\text{double}} - M_{\text{diff}}^{\text{double}} > \delta_{\text{double}}$ **then**
  $d_{\text{est}} = 1$;
else if $\mid M_{\text{same}}^{\text{double}} - M_{\text{diff}}^{\text{double}} \mid \leq \delta_{\text{double}}$ **then**
  $d_{\text{est}} = 0$;
else
  Scan in a single clockwise direction and calculate M^{single};
  if $M_{\text{same}}^{\text{double}} - M^{\text{single}} < -\delta_{\text{double}}$ **then**
    $d_{\text{est}} = -1$;
    Update $M_{\text{diff}}^{\text{double}} = M^{\text{single}}$; Exchange values of $M_{\text{same}}^{\text{double}}$ and $M_{\text{diff}}^{\text{double}}$ with each other;
  else
    $d_{\text{est}} = 0$;
  end if
end if

3.4. Movement toward the Optimal Angle

With the estimated deviation direction, the antenna beam is rotated during unidirectional scanning until it reaches the optimal angle. On the one hand, if the deviation direction does not change during unidirectional scanning, the difference between the metrics for two scanning directions, i.e., $M^{\text{single}} - M_{\text{diff}}^{\text{double}}$, will be greater than the threshold δ_{double}. On the other hand, with the same scanning direction, the difference between metrics M^{single} and $M_{\text{same}}^{\text{double}}$ will be small because angle adjustments within the two metrics make the actual angle closer to the optimal angle. If one of these two characteristics is not satisfied, there would be an intersection between the optimal and actual angles of the beam during scanning, indicating that the optimal angle has been reached and the deviation direction can be regarded as none. The detailed method for moving toward the optimal angle is described in Algorithm 2, where δ_{single} is positive and denotes the threshold used for the comparison between the metrics M^{single} and $M_{\text{same}}^{\text{double}}$, corresponding to scanning with the estimated deviation direction. It should be noted that δ_{single} and δ_{double} are two different thresholds. When using δ_{single}, the compared metrics are obtained from the same scanning directions, while they are obtained from different scanning directions when using δ_{double}. It should also be noted that Algorithm 2 is implemented based on Algorithm 1, and the outputs of Algorithm 1 are the initial inputs of Algorithm 2. After Algorithm 1 is implemented, the estimated deviation direction d_{est} is obtained, as well as the metrics $M_{\text{same}}^{\text{double}}$ and $M_{\text{diff}}^{\text{double}}$. Then, the values of these three variables are used to initialize the variables with the same names within Algorithm 2.

Algorithm 2 Movement toward the optimal angle

while $d_{\text{est}} \neq 0$ **do**
  Scan in a single direction d_{est} and calculate M^{single};
  if $M^{\text{single}} - M_{\text{diff}}^{\text{double}} > \delta_{\text{double}}$ and $\mid M^{\text{single}} - M_{\text{same}}^{\text{double}} \mid < \delta_{\text{single}}$ **then**
    Update $M_{\text{same}}^{\text{double}} = M^{\text{single}}$;
  else
    $d_{\text{est}} = 0$;
  end if
end while

Since the optimal angle is reached through scanning in a single direction and the same direction, the sounding overhead in this stage is low and the duration spent is short. Therefore, the overall sounding overhead is low, and the beam tracking can be achieved rapidly. Additionally, since the optimal angle is maintained through comparison and there is no complicated calculation, the computational overhead is lower than that of estimation meth-

ods such as MUSIC or Kalman-filter-based methods. It should be noted that the proposed beam tracking method is designed based on the monotonic characteristic of the antenna gain on the main lobe and the dominant impact of beam misalignment, so the application scenario can be extended to other communication systems with such characteristics.

4. Numerical Results

In this section, the performance of the proposed beam tracking method is validated through numerical results. The simulation parameters are listed in Table 2. The threshold δ_{double} is configured with a fixed value of 0.3, while δ_{single} is dynamic and set to $0.2 \cdot M_{\text{same}}^{\text{double}}$. The beam pattern shown in Figure 1 is used in the simulation. The beam tracking method is applied after an accurate beam alignment, i.e., the beam angles of the transmitter and receiver are aligned at the beginning. To simulate the relative motion, we assume that the transmitter is stationary at the point (0 m, 0 m) and the receiver moves from the point (1000 m, 0 m). The change in the actual beam angle is implemented by rotation with a limited speed. For the received signal, random noise is considered as a Gaussian process with zero mean. Given that the power of the received signal can be calculated within several nanoseconds, e.g., using a field-programmable gate array (FPGA) with a clock speed of hundreds of MHz, whereas the change in the received power due to motion needs hundreds of milliseconds, e.g., changing 0.001 degrees takes 580 milliseconds when the motion velocity is 30 m/s, there is enough time to obtain multiple values of the received power, which vary only due to noise. In order to ease the impact of noise on power measurement, the power of the received signal is averaged over five samples [23].

Table 2. Simulation parameters.

Parameter Name	Value
Operating frequency [GHz]	140
Transmit power [dBm]	0
Noise power spectral density [dBm/Hz]	−174
Transmission bandwidth [GHz]	10
Maximum antenna gain [dBi]	56
Antenna HPBW [degree]	0.2
Scanning step μ [degree]	0.02
Threshold ρ_0 [dB]	0.2
Threshold ρ_1 [dB]	6
Threshold δ_{double} [dB]	0.3
Threshold δ_{single} [dB]	$0.2 \cdot M_{\text{same}}^{\text{double}}$ (variable)

There are two benchmarks considered in this paper. The first benchmark applies wide-range scanning at the beginning to initialize the AoA estimation using a power-weighted method, followed by the angular velocity estimation based on the past five estimation results of the AoA. It then adopts narrow-range scanning by calculating the predicted angle based on a fixed scanning period $\triangle t$ [23]. The second benchmark is a hybrid method consisting of two tracking modes, where tracking mode 1 applies the search method within the vicinity, and tracking mode 2 predicts the optimal angle based on the changing trend. Beam training using an exhaustive search is carried out if both tracking modes are ineffective [15]. The scanning direction of tracking mode 2 is the same as the changing trend of the previously adopted beam angles; that of tracking mode 1, triggered by the failure of tracking mode 2, is opposite to this changing trend, and that of the others is set in the anticlockwise direction. The wide range is uniformly set to 0.2 degrees. Specifically, the first and second benchmarks are named the calculation-based method and the hybrid method, respectively.

First, we simulate the motion scenario with a fixed velocity, where the motion direction does not change and is perpendicular to the initial direction from the transmitter to the receiver. The total simulation time T is 30 s. Performance is evaluated in terms of the

root-mean-square error (RMSE) averaged over 500 trials of random noise. For each trial, the RMSE is defined as $\sqrt{\sum_{k=1}^{K}(\theta_k^{\text{act}} - \theta_k^{\text{opt}})^2/K}$, where $K = 3001$ is the number of time samples with equal intervals $T/(K-1)$. Figure 4 depicts the simulation results for two different motion directions. For each motion velocity, the scanning period $\triangle t$ used in the calculation-based method is set to 30 ms, and the corresponding averaged scanning speed can be obtained as $\sum_{l=1}^{L}(R_l)/L/\triangle t$, where L denotes the number of scans and R_l represents the total angular change during the l^{th} scan. Accordingly, the performance of the hybrid method and that of our proposed method are evaluated with this scanning speed. It should be noted that the scanning speeds for different motion velocities vary because the scanning ranges predicted by the calculation-based method differ. In contrast, the scanning speeds for different tracking methods are the same for each motion velocity within a specific motion direction.

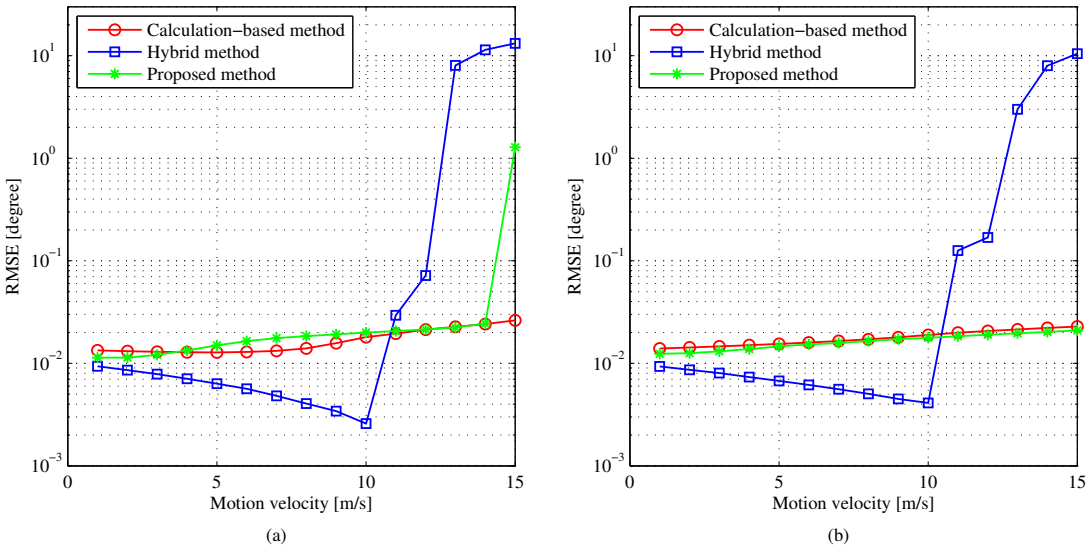


Figure 4. RMSE performance when the motion direction and velocity are fixed: (**a**) Relative angle between transmitter and receiver increases during motion. (**b**) Relative angle between transmitter and receiver decreases during motion.

As shown in Figure 4, as the relative angle between the transmitter and receiver increases during motion, the hybrid method exhibits excellent performance for motion velocities up to 10 m/s. Our proposed tracking method also performs well within this range. Similarly, the calculation-based method performs well for motion velocities up to 14 m/s but exhibits the best performance for motion velocities up to 15 m/s. In the hybrid method, when the motion velocity is low, the optimal angle can be initially reached through tracking mode 1 and subsequently predicted correctly through tracking mode 2. Since there is no searching procedure in tracking mode 2, the scanning range of the hybrid method is the smallest, and excellent performance is achieved. However, when the motion velocity is high, tracking mode 1 cannot keep up with the rapidly changing optimal angle, which restricts the scanning to the immediate vicinity. Accordingly, the changing trend of the optimal angle cannot be recognized, leading to poor performance when the motion velocity is above 10 m/s and a large RMSE difference when the motion velocity is above 12 m/s. It should be noted that with faster scanning speeds, this performance could be improved, as it would allow tracking mode 1 to remain effective at higher motion velocities. In our proposed method, although the scanning range is also restricted to the immediate vicinity, the deviation direction, rather than the AoA, is correctly identified, and accordingly, the optimal angle can be reached. Therefore, it outperforms the hybrid method when the motion velocity is high. However, this performance is restricted by the scanning speed when the motion velocity is 15 m/s. For the calculation-based method, since the motion velocity is fixed, the angular velocity estimated

using previous values converges toward the true value and is accurate for the next period, with which the range of the optimal angle can be predicted correctly even for high-speed motion, leading to the best performance when the motion velocity is 15 m/s.

When the relative angle between the transmitter and receiver decreases during motion, our proposed tracking method and the calculation-based method always exhibit similar performance, even when the motion velocity is as high as 15 m/s. Compared with the motion where the relative angle between the transceiver and receiver increases, in this case, the angular change in the narrow-range scanning applied in the anticlockwise direction in the calculation-based method is larger, leading to a higher scanning speed (3.5 degree/s compared with 1.9 degree/s), so the performance of our proposed method shows an improvement.

Second, we simulate the motion scenario with a variable direction and velocity, where the displacement versus time is modeled as a sinusoidal function, and the motion direction is vertical to the initial direction from the transmitter to the receiver. The total simulation time is 30 s, consisting of four cycles of sinusoidal motion. The simulation results are shown in Figure 5, where the averaged motion velocity is calculated by dividing the total path length by the total time spent. For each averaged motion velocity, the scanning period $\triangle t$ used in the calculation-based method is set to 30 ms, and the scanning speeds for different tracking methods remain the same. It should be noted that the scanning speeds for different motion models vary, even with the same averaged motion velocity, since the scanning ranges predicted by the calculation-based method differ. In contrast, the scanning speeds for different tracking methods are the same for each averaged motion velocity within a specific motion model.

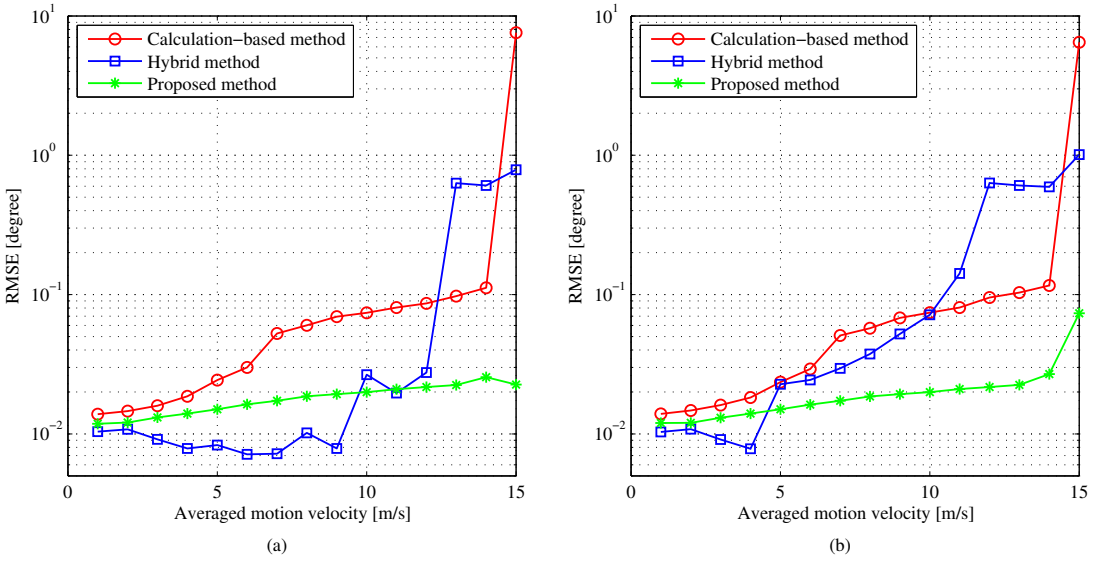


Figure 5. RMSE performance when the motion direction and velocity are variable: (**a**) Displacement versus time is modeled as a sinusoidal function. (**b**) Displacement versus time is modeled as a negative sinusoidal function.

When the motion velocity is high, our proposed method exhibits the best RMSE performance. For example, as shown on the left, when the motion velocity is 13 m/s, the RMSE of our method is only 0.02 degrees, while that of the calculation-based method is 0.10 degrees, and that of the hybrid method is 0.63 degrees. In the calculation-based method, the angular velocity used to predict the range of the optimal angle is calculated using the past estimations of the angle, but it is not accurate when the motion velocity is changed, so the performance is much poorer than the situation with a fixed motion velocity. Notably, when the averaged motion velocity is 15 m/s, due to the accumulated estimation error of the angular velocity, the predicted angle range deviates from the main lobe of the antenna, and even the whole range is located in the side lobe. Consequently, the AoA estimated using the power-weighted method is not accurate, and the estimation error of the angular

velocity becomes significant, resulting in a large alignment error. In the hybrid method, performance is excellent when the motion velocity is low due to the smallest scanning range, but it becomes inadequate when the motion velocity is high because of the ineffectiveness of the two tracking modes. Furthermore, when the displacement versus time is modeled as a negative sinusoidal function, as shown in Figure 5b, the performance of the hybrid method is worse than that shown in Figure 5a when the motion velocity ranges from 5 m/s to 10 m/s. In this case, the motion starts in a clockwise direction, while the hybrid method initiates scanning in an anticlockwise direction and then applies wide-range scanning also in an anticlockwise direction, making the duration to reach the optimal angle long. In our proposed method, the deviation direction can be correctly identified without prediction, and the optimal angle can be reached in a single direction. Therefore, its performance remains good and it outperforms the other two methods when the motion velocity is high. Also, due to the different scanning speeds, the performance of our proposed method, as shown in Figure 4, differs from that shown in Figure 5 when the motion velocity is 15 m/s. It should be noted that the averaged motion velocity at which our proposed method starts to show better performance is related to specific characteristics of motion direction and motion velocity changes. For high motion velocities, our proposed method exhibits the best performance.

Finally, we simulate the random motion scenario, where the moving direction randomly changes following a uniform distribution ranging from 0 degrees to 360 degrees, and the motion velocity randomly changes following a uniform distribution ranging from 0 m/s to 30 m/s. In order to track this random motion, the scanning period $\triangle t$ used in the calculation-based method is set to 10 ms, resulting in a corresponding scanning speed of about 8 degree/s. Figure 6 shows a tracking example over a 10 s simulation time, illustrating the variation in the beam angle due to random motion and the corresponding beam alignment error.

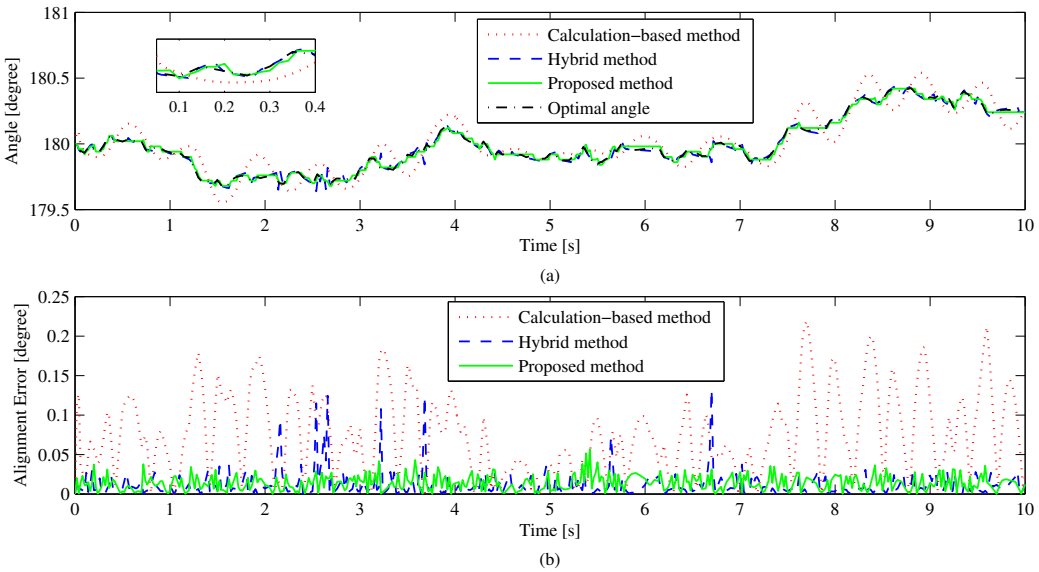


Figure 6. Tracking example for random motion: (**a**) Actual beam direction and optimal beam direction. (**b**) Beam alignment error.

In the calculation-based method, the angular velocity is estimated using past estimations of the optimal angle, which requires enough time to converge toward the true value and adapt to changes in the motion velocity. Due to the rapidly changing optimal angle, the estimated angular velocity may not be accurate, and the predicted angle range may deviate from the optimal range. Therefore, the change in the actual beam angle obtained using the calculation-based method may not align well with the change in the optimal angle, e.g., the optimal angle may start increasing at time instant 0.1 s, but the actual angle may

start increasing after 0.2 s, leading to poor RMSE performance of 0.09 degrees. In the hybrid method, the prediction of the optimal beam angle is restricted to the immediate vicinity, which may be ineffective for high motion speeds. Consequently, wide-range beam training is performed, leading to significant alignment errors during scanning and substantial estimation errors. Although only a small alignment error is obtained most of the time, there are seven instances of significant alignment errors for the hybrid method, as illustrated in Figure 6b. In our proposed method, with a small scanning range, the deviation direction is recognized in a short duration and can be updated when beam misalignment is detected. As a result, the rapidly changing optimal angle is tracked, well with the minimum RMSE values of around 0.02 degrees. In addition, the proposed method shows good stability, with the maximum alignment error during motion being the smallest, at only about 0.05 degrees.

5. Conclusions

Considering the abysmal effect of beam misalignment on terahertz communications, we propose a novel beam tracking method using power measurement. The beam status is first monitored to check whether it is aligned. If the beam is not aligned and is within the tracking range, the deviation direction is recognized, based on which the beam is rotated until it reaches the optimal angle. With the proposed method, the sounding overhead is reduced by restricting the scanning range to the immediate vicinity, and the deviation direction, rather than the AoA, is recognized without prediction. When the motion velocity is high, the deviation direction can be correctly identified within this small scanning range, while the AoA obtained using the traditional beam search method may not catch up with the rapidly changing optimal angle. Furthermore, unlike the prediction algorithm, the scanning range is narrowed down without prediction, and the deviation direction is recognized without relying on past estimations, so our proposed method can work well for variable motion. Simulation results verify the performance of our proposed method in terms of the alignment error. Its technical superiority is especially dominant in situations involving variable motion at high speeds, with competitively low and stable alignment errors.

Author Contributions: Conceptualization, X.H., C.Z., and X.Y.; methodology, X.H. and C.Z.; software, X.H.; validation, X.H.; formal analysis, X.H.; investigation, X.H.; resources, X.Y.; data curation, X.H.; writing—original draft preparation, X.H.; writing—review and editing, X.H., C.Z., and C.L.; visualization, X.H. and C.Z.; supervision, C.Z.; project administration, C.Z.; funding acquisition, C.Z. All authors have read and agreed to the published version of the manuscript.

Funding: This research was funded by the National Key Research and Development Program of China under grant No. 2021YFB2800800 and the Natural Science Foundation of Zhejiang Province under grant No. LQ21F010002.

Data Availability Statement: Data are contained within the article.

Conflicts of Interest: The authors declare no conflicts of interest.

References

1. Akyildiz, I.F.; Han, C.; Hu, Z.; Nie, S.; Jornet, J.M. Terahertz Band Communication: An Old Problem Revisited and Research Directions for the Next Decade. *IEEE Trans. Commun.* **2022**, *70*, 4250–4285. [CrossRef]
2. Chen, Z.; Han, C.; Wu, Y.; Li, L.; Huang, C.; Zhang, Z.; Wang, G.; Tong, W. Terahertz Wireless Communications for 2030 and Beyond: A Cutting-Edge Frontier. *IEEE Commun. Mag.* **2021**, *59*, 66–72. [CrossRef]
3. He, Y.; Sheng, B.; Li, Z. Channel Modeling Based on Transformer Symbolic Regression for Inter-Satellite Terahertz Communication. *Appl. Sci.* **2024**, *14*, 2929. [CrossRef]
4. Sarieddeen, H.; Alouini, M.S.; Al-Naffouri, T.Y. An Overview of Signal Processing Techniques for Terahertz Communications. *Proc. IEEE* **2021**, *109*, 1628–1665. [CrossRef]
5. Petrov, V.; Moltchanov, D.; Koucheryavy, Y.; Jornet, J.M. Capacity and Outage of Terahertz Communications with User Micro-Mobility and Beam Misalignment. *IEEE Trans. Veh. Technol.* **2020**, *69*, 6822–6827. [CrossRef]
6. Dabiri, M.T.; Hasna, M.; Zorba, N.; Khattab, T.; Qaraqe, K.A. A General Model for Pointing Error of High Frequency Directional Antennas. *IEEE Open J. Commun. Soc.* **2022**, *3*, 1978–1990. [CrossRef]
7. Kokkoniemi, J.; Boulogeorgos, A.A.A.; Aminu, M.; Lehtomäki, J.; Alexiou, A.; Juntti, M. Impact of beam misalignment on THz wireless systems. *Nano Commun. Netw.* **2020**, *24*, 100302. [CrossRef]

8. Attaoui, W.; Bouraqia, K.; Sabir, E. Initial Access & Beam Alignment for mmWave and Terahertz Communications. *IEEE Access* **2022**, *10*, 35363–35397.
9. Chen, Y.; Yan, L.; Han, C. Millidegree-Level Direction-of-Arrival (DoA) Estimation and Tracking for Terahertz Wireless Communications. In Proceedings of the 2020 17th Annual IEEE International Conference on Sensing, Communication, and Networking (SECON), Como, Italy, 22–25 June 2020.
10. Wang, Z.; Xie, W.; Zou, Y.; Wan, Q. DOA Estimation Using Single or Dual Reception Channels Based on Cyclostationarity. *IEEE Access* **2019**, *7*, 54787–54795. [CrossRef]
11. Matsuno, H.; Nagao, T.; Amano, Y. Angle Estimation of Wireless Device Using Power Weighted Average Angle for Virtulized Terminal Using THz Band. In Proceedings of the 2022 IEEE International Symposium on Antennas and Propagation and USNC-URSI Radio Science Meeting (AP-S/URSI), Denver, CO, USA, 10–15 July 2022.
12. Chen, Y.; Yan, L.; Han, C.; Tao, M. Millidegree-Level Direction-of-Arrival Estimation and Tracking for Terahertz Ultra-Massive MIMO Systems. *IEEE Trans. Wirel. Commun.* **2022**, *21*, 869–883. [CrossRef]
13. Cousik, T.S.; Shah, V.K.; Erpek, T.; Sagduyu, Y.E.; Reed, J.H. Deep Learning for Fast and Reliable Initial Access in AI-Driven 6G mm Wave Networks. *IEEE Trans. Netw. Sci. Eng.* 2022, *early access* . [CrossRef]
14. Khalili, A.; Rangan, S.; Erkip, E. On Single-User Interactive Beam Alignment in Next Generation Systems: A Deep Learning Viewpoint. In Proceedings of the 2021 IEEE International Conference on Communications Workshops (ICC Workshops), Montreal, QC, Canada, 14–23 June 2021.
15. Ning, B.; Chen, Z.; Tian, Z.; Han, C.; Li, S. A Unified 3D Beam Training and Tracking Procedure for Terahertz Communication. *IEEE Trans. Wirel. Commun.* **2022**, *21*, 2445–2461. [CrossRef]
16. Lin, C.; Li, G.Y.; Wang, L. Subarray-Based Coordinated Beamforming Training for mmWave and Sub-THz Communications. *IEEE J. Sel. Areas Commun.* **2017**, *35*, 2115–2126. [CrossRef]
17. Wu, Y.; Koch, J.; Vossiek, M.; Gerstacker, W. Hierarchical Beam Alignment in Single-User MIMO Single-Carrier Frequency Division Multiple Access Terahertz Communication Systems. In Proceedings of the 2021 IEEE International Conference on Communications Workshops (ICC Workshops), Montreal, QC, Canada, 14–23 June 2021.
18. Liu, X.; Yu, J.; Qi, H.; Yang, J.; Rong, W.; Zhang, X.; Gao, Y. Learning to Predict the Mobility of Users in Mobile mmWave Networks. *IEEE Wirel. Commun.* **2020**, *27*, 124–131. [CrossRef]
19. Huang, Y.; Wu, Q.; Lu, R.; Peng, X.; Zhang, R. Massive MIMO for Cellular-Connected UAV: Challenges and Promising Solutions. *IEEE Commun. Mag.* **2021**, *59*, 84–90. [CrossRef]
20. Karaçora, Y.; Chaccour, C.; Sezgin, A.; Saad, W. Event-Based Beam Tracking With Dynamic Beamwidth Adaptation in Terahertz (THz) Communications. *IEEE Trans. Commun.* **2023**, *71*, 6195–6210. [CrossRef]
21. Huang, Y.; Wu, Q.; Wang, T.; Zhou, G.; Zhang, R. 3D Beam Tracking for Cellular-Connected UAV. *IEEE Wirel. Commun. Lett.* **2020**, *9*, 736–740. [CrossRef]
22. Shahsavari, S.; Amir Khojastepour, M.A.; Erkip, E. Robust Beam Tracking and Data Communication in Millimeter Wave Mobile Networks. In Proceedings of the 2019 International Symposium on Modeling and Optimization in Mobile, Ad Hoc, and Wireless Networks (WiOPT), Avignon, France, 3–7 June 2019.
23. Matsuno, H.; Nagao, T.; Hayashi, T. High-Accuracy and High-Speed Beam Tracking Algorithm for THz Short-Range Mobile Communication. In Proceedings of the 2023 17th European Conference on Antennas and Propagation (EuCAP), Florence, Italy, 26–31 March 2023.
24. Gao, X.; Dai, L.; Zhang, Y.; Xie, T.; Dai, X.; Wang, Z. Fast Channel Tracking for Terahertz Beamspace Massive MIMO Systems. *IEEE Trans. Veh. Technol.* **2017**, *66*, 5689–5696. [CrossRef]
25. Zhao, J.; Gao, F.; Jia, W.; Zhang, S.; Jin, S.; Lin, H. Angle Domain Hybrid Precoding and Channel Tracking for Millimeter Wave Massive MIMO Systems. *IEEE Trans. Wirel. Commun.* **2017**, *16*, 6868–6880. [CrossRef]
26. Stratidakis, G.; Ntouni, G.D.; Boulogeorgos, A.A.; Kritharidis, D.; Alexiou, A. A Low-Overhead Hierarchical Beam-tracking Algorithm for THz Wireless Systems. In Proceedings of the 2020 European Conference on Networks and Communications (EuCNC), Dubrovnik, Croatia, 15–18 June 2020.
27. Zhang, W.; Zhang, W.; Wu, J. UAV Beam Alignment for Highly Mobile Millimeter Wave Communications. *IEEE Trans. Veh. Technol.* **2020**, *69*, 8577–8585. [CrossRef]
28. Lim, S.H.; Kim, S.; Shim, B.; Choi, J.W. Efficient Beam Training and Sparse Channel Estimation for Millimeter Wave Communications Under Mobility. *IEEE Trans. Commun.* **2020**, *68*, 6583–6596. [CrossRef]
29. Li, J.; Sun, Y.; Xiao, L.; Zhou, S.; Sabharwal, A. How to Mobilize Mmwave: A Joint Beam and Channel Tracking Approach. In Proceedings of the 2018 IEEE International Conference on Acoustics, Speech and Signal Processing (ICASSP), Calgary, AB, Canada, 15–20 April 2018.
30. Song, H.L.; Ko, Y.C. Robust and Low Complexity Beam Tracking With Monopulse Signal for UAV Communications. *IEEE Trans. Veh. Technol.* **2021**, *70*, 3505–3513. [CrossRef]
31. Zhang, J.; Huang, Y.; Zhou, Y.; You, X. Beam Alignment and Tracking for Millimeter Wave Communications via Bandit Learning. *IEEE Trans. Commun.* **2020**, *68*, 5519–5533. [CrossRef]
32. Xue, Q.; Ji, C.; Ma, S.; Guo, J.; Xu, Y.; Chen, Q.; Zhang, W. A Survey of Beam Management for mmWave and THz Communications Towards 6G. *IEEE Commun. Surv. Tutor.* **2024**, *early access*. [CrossRef]

33. Shi, J.; Li, M.; Tang, L.; Li, X.; Jia, X.; Guo, C.; Bai, H.; Ma, H.; Wang, X.; Niu, P.; et al. All-Dielectric Integrated Meta-Antenna Operating in 6G Terahertz Communication Window. *Small* **2024**, *20*, 2308958. [CrossRef]
34. Beiranvand, B.; Sobolev, A.S. Resonant-wavelength tuning of a fibonacci one dimensional photonic crystal filter at telecommunication wavelengths. *Optik* **2021**, *240*, 166926. [CrossRef]
35. Lin, Z.; Wang, L.; Ding, J.; Xu, Y.; Tan, B. Tracking and Transmission Design in Terahertz V2I Networks. *IEEE Trans. Wirel. Commun.* **2023**, *22*, 3586–3598. [CrossRef]
36. Yan, L.; Han, C.; Yuan, J. A Dynamic Array-of-Subarrays Architecture and Hybrid Precoding Algorithms for Terahertz Wireless Communications. *IEEE J. Sel. Areas Commun.* **2020**, *38*, 2041–2056. [CrossRef]
37. Datasheet of Anteral's Cassegrain Reflector Systems CRS-520-WRxx. Available online: https://anteral.com/products/antenna-passives/cassegrain-reflector-systems-ra-dc-d-f/ (accessed on 10 April 2023).

Disclaimer/Publisher's Note: The statements, opinions and data contained in all publications are solely those of the individual author(s) and contributor(s) and not of MDPI and/or the editor(s). MDPI and/or the editor(s) disclaim responsibility for any injury to people or property resulting from any ideas, methods, instructions or products referred to in the content.